Comparison of GPI turbulence seen in the Phantom camera and APD array

sz and jt
5/3/15

This note describes a comparison between the GPI turbulence seen by the midplane Phantom 710 camera and the APD array at the midplane. These two detectors view the same GPI gas puff, but with different viewing angles, spatial resolutions, and bandwidths. The Phantom 710 camera views the puff at an 11º vertical angle aligned along a typical B field line, and the APD array views purely toroidally. The camera data has 64x64 pixels digitized at 400 kHz, and the APD has 9x10 channels (some dead) digitized at 2 MHz. The APDs have better signal/noise levels.

The turbulence analysis is done with exactly the same methods for both detectors using: /home/zweben/APD/cam_apd_comp_10.pro. This analysis is based on the cross-detector space and time alignment done found in: /home/zweben/APD/cam_apd_11.pro. The subsets of Phantom data used for this analysis is read from the large camera data files for each shot and time and saved using: /home/zweben/APD/710_velcor_apd.pro.

1. Spatial alignment

The locations of the camera pixels and APD channels in the (R,z) plane are shown in Fig. 1 based on the in-vessel registration done by Jim in 2015. This corrects an earlier mis-registration of the camera used for the 2010-2012 runs, which was off by a few mm. This actual physical spatial alignment is the same for all of GPI data from 2010-2015.

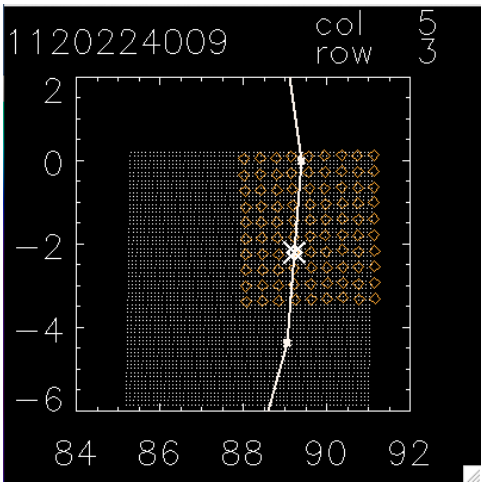

Fig. 1 – spatial alignment of APDs diodes (orange) and camera pixels (white dots), with separatrix in white line. Column 0 is at the right, 8 at left, row 0 at bottom, row 9 at top.

2. Timing alignment

There was a systematic ~28-38 μsec delay between the timing of the Phantom camera and the timing of the APD data, due to the internal clock of the Phantom, which is internally running after initial triggering in each shot (the APDs time is monitored using absolute timing pulses, as in Stillerman FED '10). The timing re-alignment for each cross-comparison for each shot was done using the GPI turbulence data itself by finding the time delay needed to get the maximum cross-correlation between an APD and the nearest Phantom camera pixel. The results are shown in Fig. 2 for all the cross-comparisons used in this note. There is no systematic variation of the derived lag time with the maximum cross-correlation coefficient, which means that the correlations were all high enough to find the time lag. The derived time lag was very nearly constant for all cross-comparisons within a single shot, as expected.

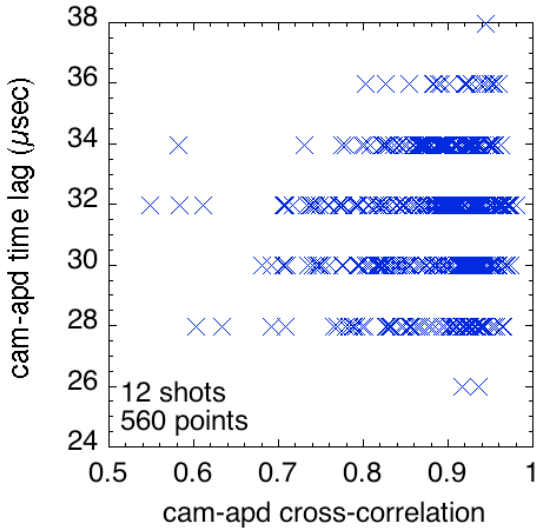

Fig. 2 – cross-correlation vs. lag times

3. Shots, times, and database

This analysis used 12 shots from 2012 run for cross-comparisons as listed in Table 1. The first 9 of these were from the shot list used for the "midplane-X-region" camera comparison (Zweben et al, PoP 2013), and the final three were suggested by Jim. The times of interest were chosen to be in the steady-state part of the discharge with no transients such as ELMS or L-H transitions. The duration of the time series for all the comparisons was taken to be 2 msec, which was enough to get good statistics for the turbulence analysis. For each shot the APDs in the range from col #1-6 were analyzed (i.e. not including col 0 on the large-R side, or columns 7-8 on the low-R side inside the separatrix where the camera signals were noisy), and rows #1-8 (i.e. not at the top and bottom edges of the array), and columns #5 and #6 were skipped for some shots with small outer gaps. This led to 560 separate cross-comparisons between APDs can camera pixels, as shown in Fig. 2.

Table 1: shot list

Shot	start (sec)	Ip	Bt	cols	sep col
1120224009	0.710	0.9	4.6	1-6	5
1120224015	0.812	1.0	6.0	1-5	5
1120224022	1.046	1.0	5.2	1-6	5
1120224023	1.140	1.0	5.2	1-6	5
1120224024	1.132	1.0	5.2	1-6	5
1120712026	1.442	0.73	4.2	1-5	2
1120712027	1.442	0.73	4.2	1-4	2
1120815018	1.270	0.9	5.6	1-6	5
1120815030	1.260	0.91	5.6	1-6	6
1120711021	1.402	0.8	5.4	1-6	4
1120731018	1.265	0.9	5.6	1-4	4
1120905002	0.862	0.8	5.4	1-6	8

4. Data preparation

The data preparation was done in /home/zweben/apd/apd_cam_11.pro, with the APDs prepared in the first part of this code by /home/terry/gpi/APDs/apd_movie.pro. Time series of 2 msec duration were found for each APD and camera pixel. The APD backgrounds were subtracted and the dead APD pixels were replaced with the average of the nearest-neighbor pixels. Each APD signal was normalized to its time-average over the period of interest, and each normalized APD time series was re-binned into a 1000 frame times series using "congrid,/interp". The camera data was smoothed over 3x3 pixels in space and re-binned into a 1000 frame times series using "congrid,/interp". The cross-correlation between each APD and the nearest camera pixel in space (from Fig. 1) was done using a variable time lag. The time lag for maximum cross-correlation was found and the time series of the APDs were adjusted to match the camera. The resulting comparison of signals vs. time is shown in Fig. 4. Here the APS pixel col/row=4/4 is compared with the camera pixel 47/42 for shot 1120224009. The cross-correlation between these two signals was 0.936 for this case, which was relatively high.

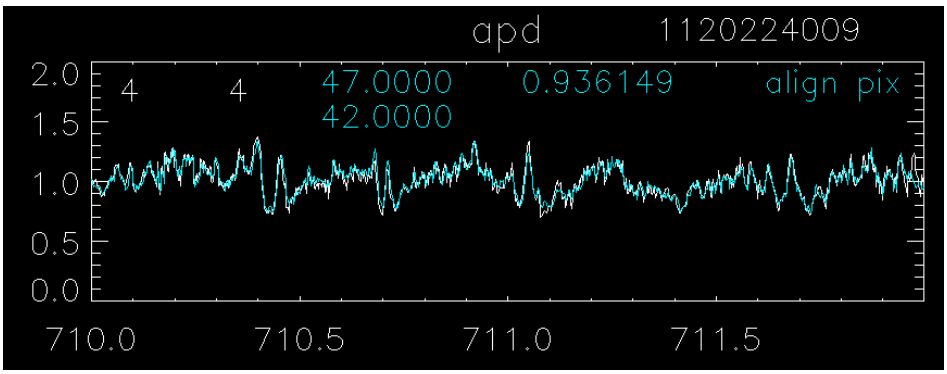

Fig. 3 – APD (blue) vs. nearest camera pixel (white)

Examples of four consecutive 2D images of the camera vs. APD are shown in Fig. 4, with the location and relative size of the arrays shown approximately to scale. Note that the relative APD signals are obtained from the output of Jim's code /home/terry/gpi/APDs/apd_movie.pro. The number of pixels in these images were expanded by x5 for the camera data and x10 for the APD data and interpolated using "congrid". The left region of the camera image was set to black due to low signal levels. There is a clear similarity between the camera and APD images, and a clear similarity in the motion of the structures, as seen in the movie in apd_cam_comp_10.pro.

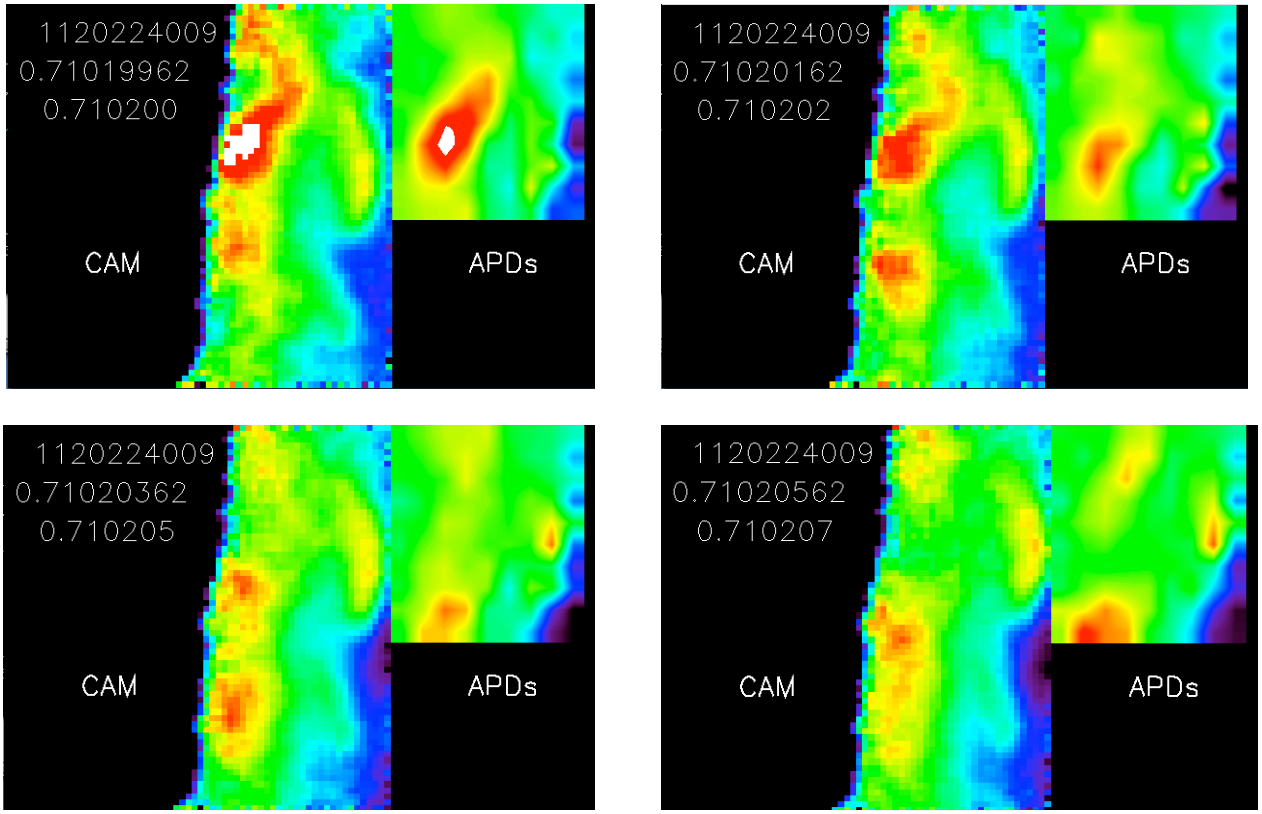

Fig. 4 - frames from the camera (left) and APD (right) arrays for 4 consecutive times separated by about 2 msec. The images are similar within the common spatial range.

5. Cross-correlation maps and radial profiles

Maps of the cross-correlation coefficient between the APDs and the nearest camera pixel are shown in Fig. 5 for two shots over the 9x10 (interpolated) APD array. In the left shot (1120224009) the cross-correlation falls of substantially in the low-R regions well inside the separatrix, due to low signal/noise in this region of Phantom data. At the right (1120905002) the separatrix is near the left-most APD pixel and the correlation is high (red) almost everywhere.

The radial profile of cross-correlation coefficient for the 560 APD points used in this study is shown in Fig. 6 as a function of the closest distance to the separatrix. The

correlation is generally lower inside the separatrix than outside due to the lower signal/noise levels, especially in the camera data. Outside the separatrix (408/560 points) the average cross-correlation between APD and camera was 0.91.

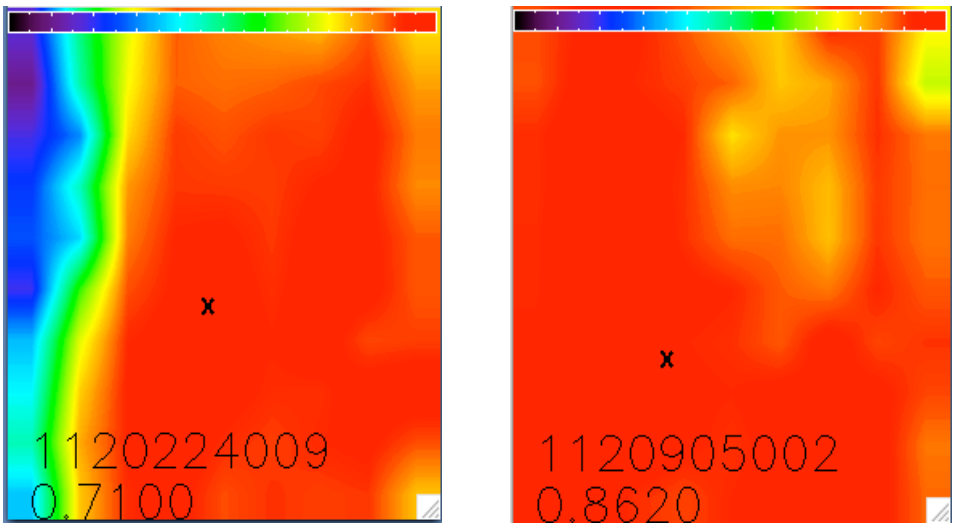

Fig. 5 - correlation of APD and camera over the APD array (interpolated). The color scale is shown from 0 to 1 at the top

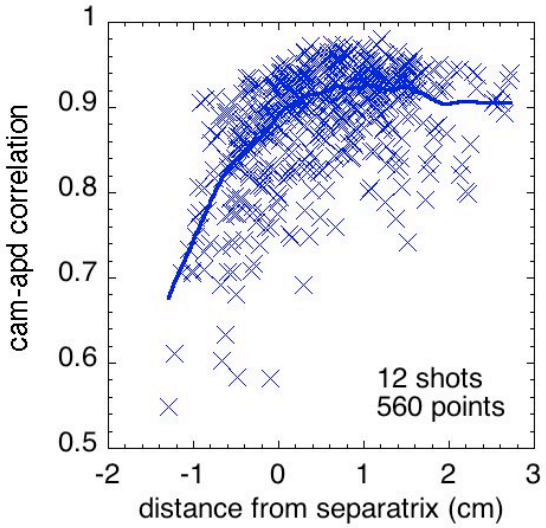

Fig. 6 – cross-correlation coefficient vs. radius with respect to the local separatrix. The correlation is reduced inside the separatrix, and the average correlation outside the separatrix is 0.91.

6. Turbulence comparisons

This part describes comparisons of the turbulence results for the APDs vs. the camera for data points with a cross-correlation coefficient of ≥0.9 between the APD and the nearest camera pixel. This level was (arbitrarily) chosen to avoid difference due to low cross-correlation, which is mainly associated with low signal levels in the camera. There were 314/560 points in the database which satisfied this criterion over the range from -1 inside to +3 cm outside the separatrix.

A. Relative fluctuation levels

The relative fluctuation level (standard deviation divided by the mean) of the APD and camera data for all the points with ≥0.9 cross-correlation coefficient is shown in Fig. 7 vs. radius (left) and vs. each other (right). The average ratio of APD/cam = 1.24±0.23. Thus on average the APDs have nearly the same fluctuation level as the camera data, to within error bars. Note that both Phantom and APD signals were effectively smoothed to the same bandwidth using "congrid", as described in Sec. 4.

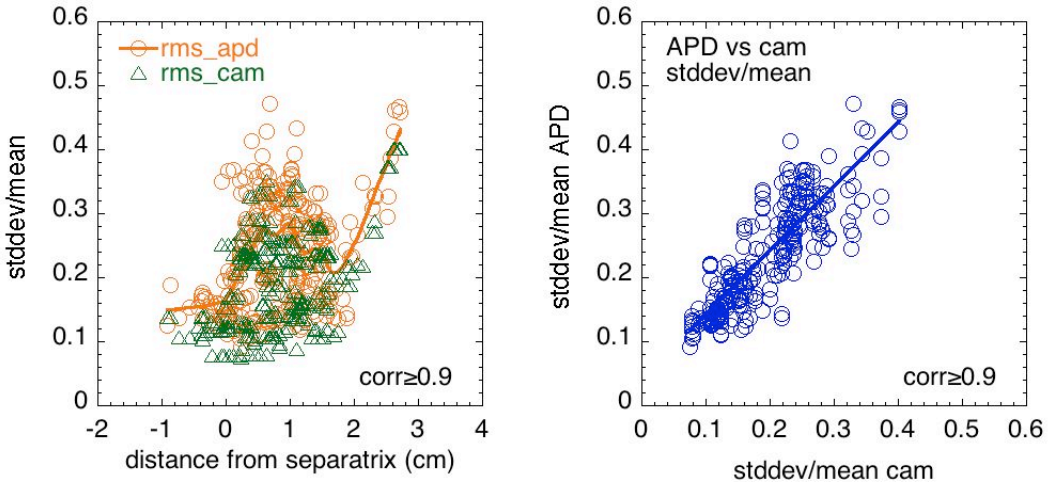

Fig. 7 – relative fluctuation levels

B. Autocorrelation times

The autocorrelation times (FWHM) vs. radius are shown in Fig. 7 (left) and vs. each other (right), calculated using "a_correlate". The ratio of these two times APD/cam =1.14±0.5. These are the same to within the uncertainties, but it is surprising that the ratio of these has such a wide variation for these data with high cross-correlation. The correlation time of ≥100 μsec are unusual and mostly come from the last two shots in Table 1, with a few from 1120712026,027 (the shots with small outer gaps).

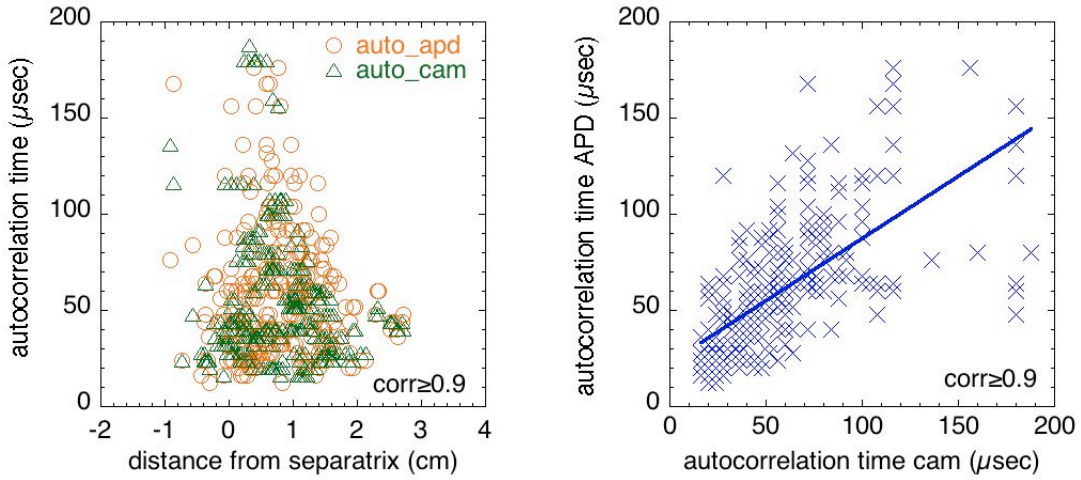

Fig. 8 – autocorrelation times (FWHM) vs. radius and each other.

C. 2D spatial cross-correlation functions

The 2D zero-time-delay spatial cross-correlation functions starting from a typical APD point (4,4) and the corresponding camera pixel (47,42) are shown in Fig. 9, with approximately the relative size and location of these arrays. The images at the top are in their original pixel formats (64x64 for the camera and 9x10 for the APDs), and the images at the bottom were re-binned and interpolated for higher spatial resolution using "congrid" (camera pixels by 5x and APD diodes by10x). These images show a similar spatial structure of the 2-D correlation function, but seem to have a slightly different tilt angle (see below). The color scale is the same as for Fig. 5, with green = 0.5 correlation. A similar result was described in I. Czeigler's thesis (in discussion of Fig. 4-7).

D. Poloidal correlation lengths

The poloidal correlation lengths as shown in Fig. 10 for the APD and camera data were found by cross-correlating vertical rows of the 2D expanded correlation functions such as at the bottom of Fig. 9, and finding the FWHM of the resulting correlation functions. If these channels were near the top and bottom edges of the arrays, the correlation functions did not cross 0.5 on both sides, and no poloidal correlation length was determined for that point. The cases with unusually large Lpol ≥3 cm were mostly from the last 2 shots in Table 1 and 1120224023 and 024. There were only 108 data points in the APD-cam comparison, in which the ratio of 0.71±0.1. Thus the APDs had a significantly smaller poloidal correlation length than the corresponding camera data for cases with ≥0.9 cross-correlation.

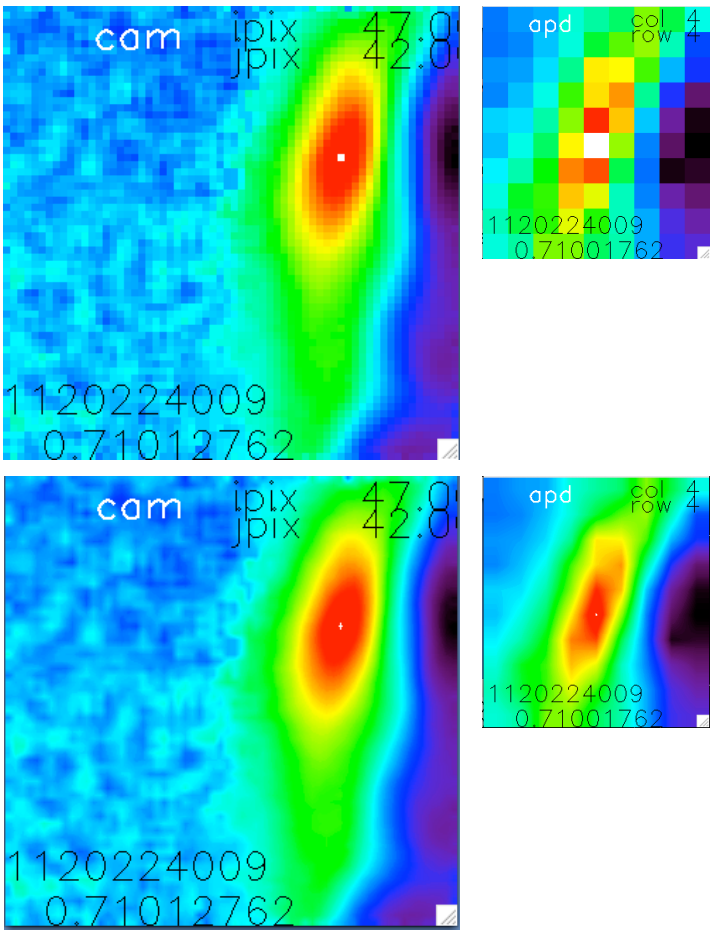

Fig. 9 – 2D cross spatial correlation functions of the camera (left) and APD array (right). The top are in original format and the bottom are re-binned by x5 (cam) and x10 (APD).

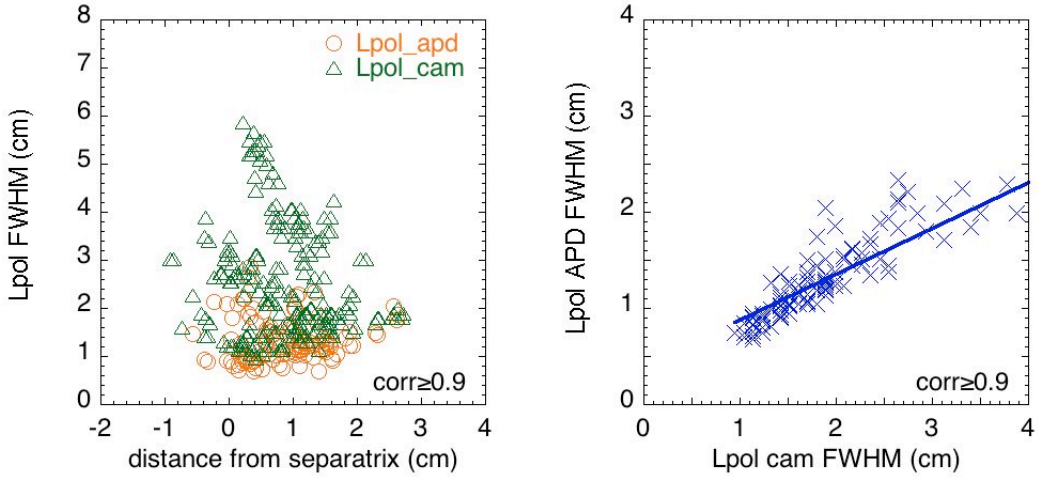

Fig. 10 – Poloidal correlation lengths (FWHM) vs. radius (left) and APD vs cam (right).

E. Radial correlation lengths

The radial correlation lengths vs. radius and APD vs. cam are shown in Fig. 11. The Lrad radio of APD/cam is 0.66±0.1, even smaller than for Lpol. There were 111 points in the APD vs. cam comparison of Fig. 11.

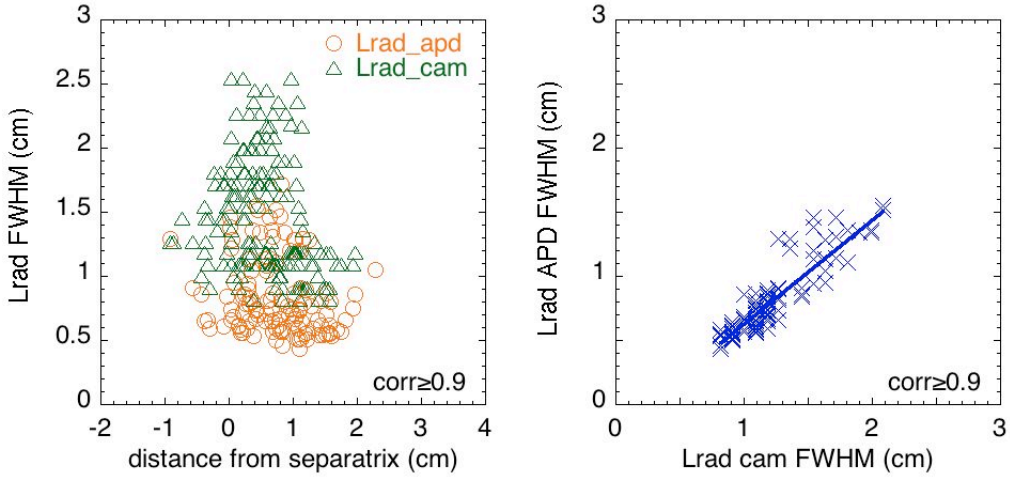

Fig. 11 - Radial correlation length comparison

F. Poloidal and radial velocity

The poloidal and radial velocities were found for each APD and its corresponding nearest camera pixel using time-delayed cross-correlation analysis, essentially the same as described in Zweben et al, PoP 2013. The velocity analysis was based on the x5 (cam) or x10 (APD) pixel-expanded and interpolated data frames such as shown in Fig. 4. The location in space of the pixel with the maximum cross-correlation with the starting pixel's time series after a variable time-frame delay was found by searching over the whole array. The poloidal and radial locations of points with ≥ 0.7 cross-correlation coefficient after 1-6 frames delay time were fit by a straight line, and the poloidal and radial velocity was found from a linear fit to the spatial displacement vs. time.

The resulting poloidal and radial velocities vs. radius and each other are shown in Fig. 12. There is a fairly clear correlation between the poloidal velocities of the camera and APD data, but a less clear correlation of the radial velocities. The ratio of the poloidal velocities was APD/cam = 0.67 (241 points), and this ratio for the radial velocities was 0.83 (218 points). The zero velocity cases for the camera points were excluded for these ratios. It is surprising that these signals which are well correlated between the APD and Phantom result, on average, in a significantly different poloidal velocity for the two.

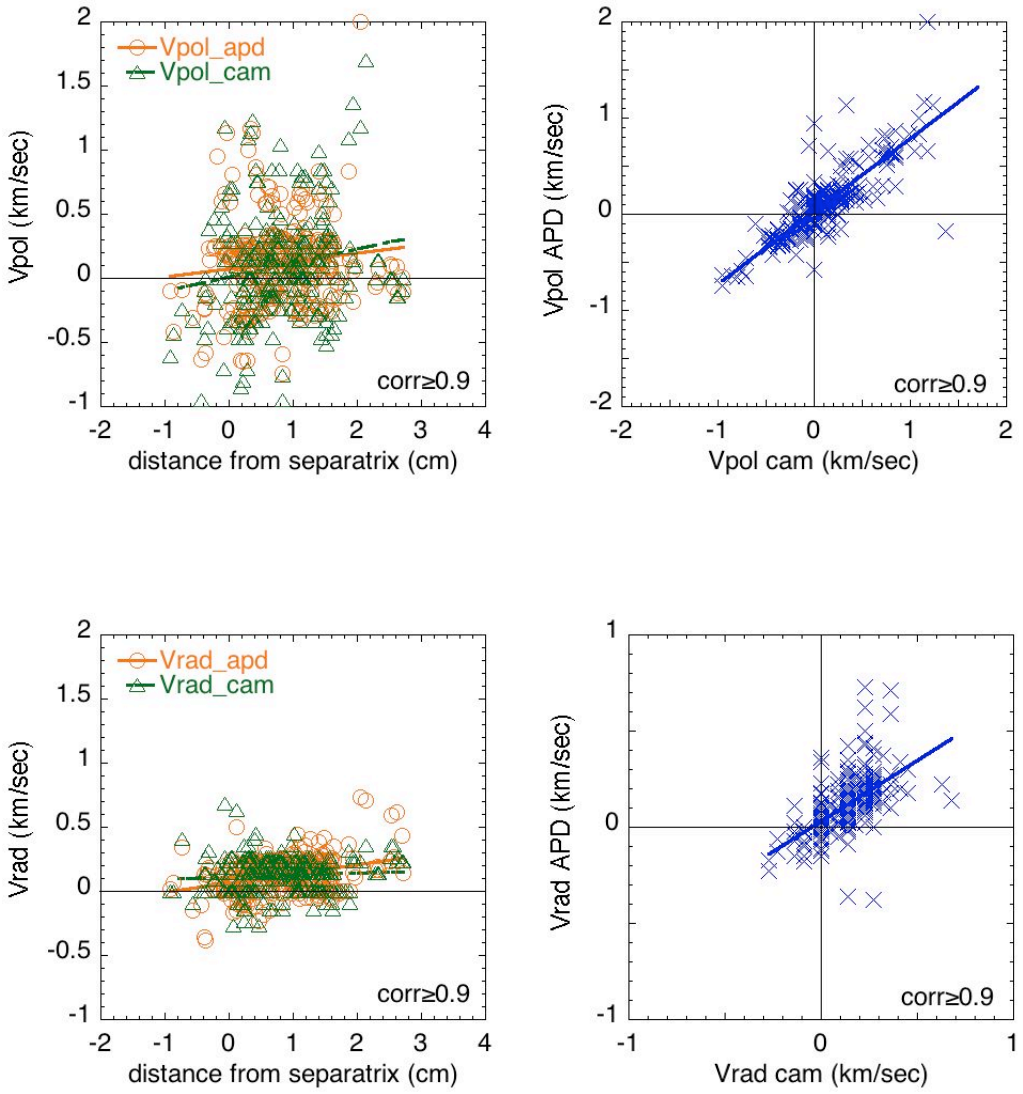

Fig. 12 – comparison of the APD and camera poloidal (top) and radial (bottom)

G. Elliptical fits to spatial correlation function

A separate method was used to compare the spatial cross-correlation functions of the APD and camera data by fitting these 2D functions with an ellipse, as illustrated in Fig. 13. The location of points in this plane at a correlation level of 0.7±0.005 were first identified (white points) and then an ellipse was fit to these (blue ellipse). This fit was done using a PPPL code by Bill Davis: /home/zweben/APD/fcfitellipse.pro; this ellipse was not constrained to be centered at the starting point for correlations. The semi-major and minor axes were evaluated as "long" and "short", their ratio is the ellipticity "ellip", and 'tilt" is the angle of the ellipse with respect to vertical (positive clockwise). Many of the fits at the edges of the arrays had unusually high ellipticity, so all fits with ellip ≥ 5 and their associated tilt angles were removed from the database.

Fig. 14 shows the ellipticity and tilt angle vs. radius and with respect to each other. The ellipticities tend to be significantly higher for the APDs. Many of the tilt angles are close to each other, but there is a wide scatter in some of the results.

Fig. 15 shows a comparison of the long and short ellipse axes for the APDs and camera. These are fairly well correlated with each other. Note that these are the half-axes at a 0.7 correlation level, so the absolute lengths are shorter than the FWHM lengths of Figs. 10 and 11.

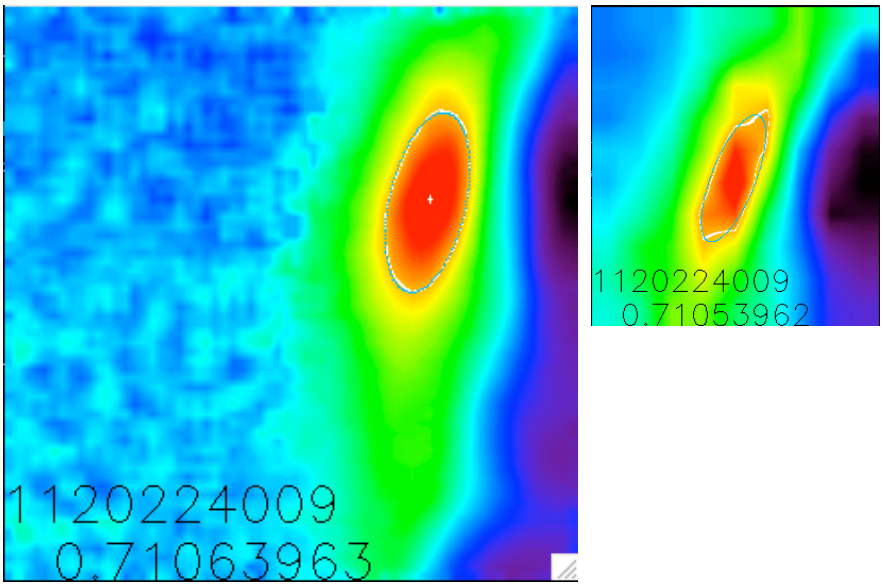

Fig. 13 – spatial cross-correlation functions of camera (left) and APD (right) fit by ellipses at a level of 0.7 correlation coefficient (black ellipse)

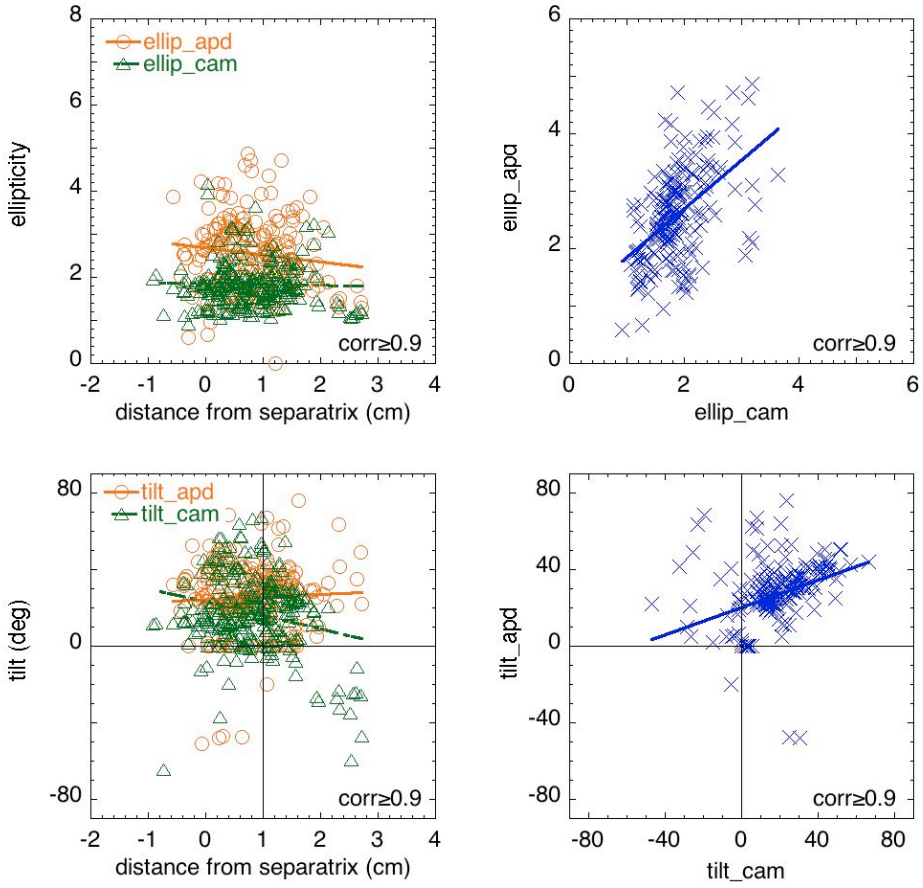

Fig. 14 – ellipticities and tilt angles of spatial cross-correlation functions

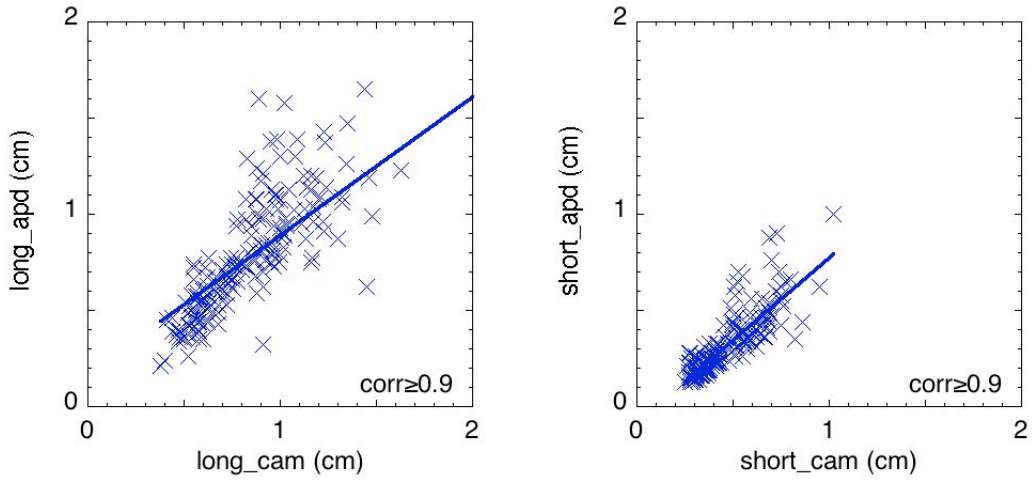

Fig. 15 - long and short ellipse axes for APD and camera

H. Summary of results

Table 2 gives a summary of the results of these comparisons. The APD/cam column shows the ratio of APD/cam for this quantity, the linear slope and linear correlations come from a linear fit of the APD vs. camera data.

In general, all of these APD/cam ratios are within 0.5-2.0. The closest results are for the normalized fluctuation level (std/mean). The correlation lengths and poloidal velocities for the APDs are about 0.7 of the camera, and the ellipticity is significantly larger for the APDs. There is a wide scatter in the results for the autocorrelation times, radial velocities, and tilt angles.

Table 2 – summary of APD/cam turbulence comparisons

quantity	# points	APD/cam	linear slope	linear correlation
std/mean	314	1.24±0.2	1.00	0.85
auto time	314	1.14±0.5	0.65	0.64
Lpol	108	0.71±0.1	0.48	0.85
Lrad	111	0.66±0.1	0.81	0.92
Vpol	241	0.67±0.1	0.76	0.83
Vrad	218	0.83±0.7	0.63	0.59
ellip	191	1.43±0.4	0.84	0.50
tilt	189	0.65±6.0	0.36	0.35
long	185	0.92±0.2	0.72	0.73
short	185	0.67±0.2	0.86	0.83

7. Interpretation of results

If the main difference between these two arrays is the viewing angle, the main expected difference would be an increase in the poloidal correlation length in the APD array, since it would be viewing the (presumably) B-field-aligned filaments at an ~11º vertical angle (depending on the assumed size of the gas cloud). This is not what the results of Fig. 10 and Table 2 show; in fact, the APD/cam Lpol ratio was 0.71 and the linear fit ratio was 0.48, i.e. the poloidal correlation decreased in the APD array. For this viewing angle effect, no significant difference would be expected on Lrad, yet the APD/cam ratio for Lrad was also 0.66, i.e. a smaller result in the APDs.

Table 3 below is reproduced from Zweben et al PoP 2009, in which the GEMR code results ("None") were smoothed to simulate the effect of the diode viewing area ("diode"), and then the added effect of the diode viewing angle ("Total"). The biggest changes due to the viewing angle were a 33% increase in Lpol and a 60% increase in Vpol. The effect of the viewing angle on Vpol was not understood at that time, but the results from Table 2 show a decrease in Vpol in the APD array compared to the camera, not an increase as expected.

TABLE III. Smoothing of GEMR (3.8 T high n case).

Parameter	None	Diode	Total
L_{pol} (cm)	0.70	0.94	1.25
L_{rad} (cm)	0.47	0.63	0.66
τ_{auto} (μs)	9.6	12.1	12.6
$\delta D_\alpha / D_\alpha$ (%)	9	8	7
V_{pol} (km/s)	0.90	1.0	1.6
V_{rad} (km/s)	0.67	0.79	0.64

One possible cause for this discrepancy might be the imperfect cross-correlation between the APD and camera time series. Fig. 16 shows the APD/cam ratio for Lpol and Vpol vs. the cross-correlation coefficient for that point over the whole database. However, there is no systematic increase in APD/cam Lpol ratio with increasing correlation; in fact, there is a slight decrease. The APD/cam Vpol ratio has a wide scatter which is not varying significantly with the correlation coefficient.

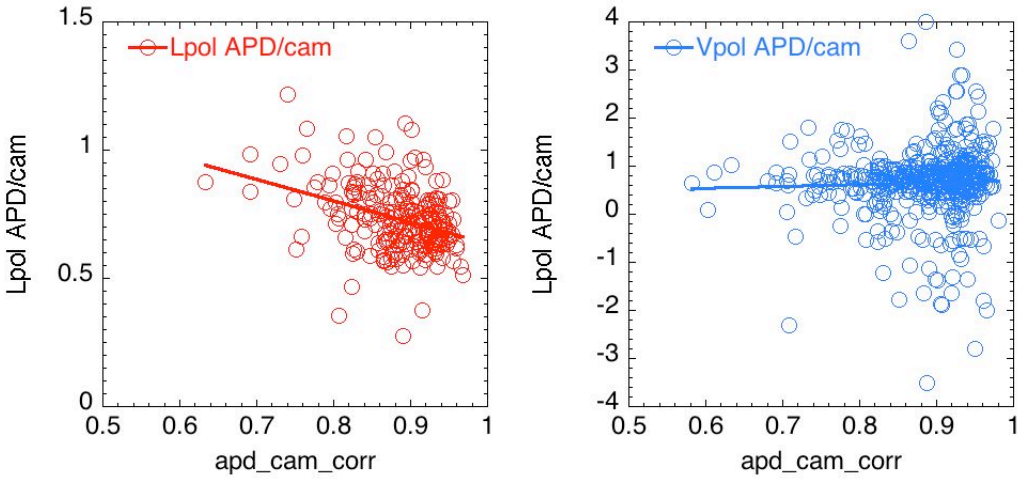

Fig. 16 – APD/cam ratios for Lpol and Vpol vs. apd-cam cross-correlation

It would be interesting to see a variation in the APD/cam ratios with the viewing angle. However, there was relatively little variation in (I/B) within the shots in this database, and there seems to be no significant variation in the L_{pol} or L_{rad} APD/cam ratios with I/B (as a proxy for viewing angle), as shown in Fig. 17. A similar result was found in I. Czeigler's thesis.

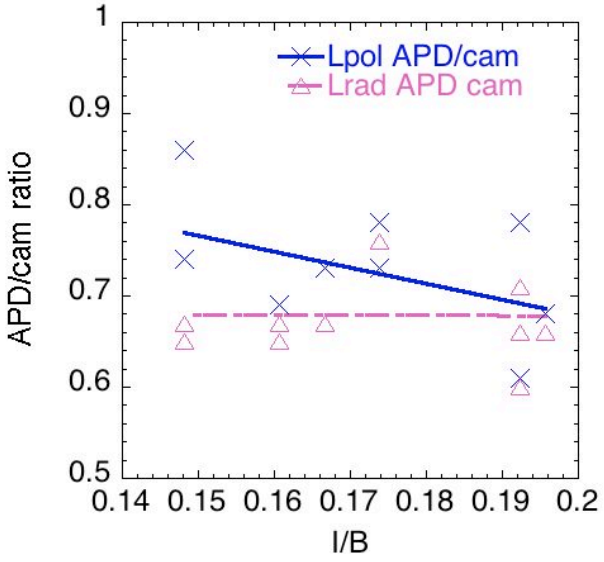

Fig. 17 – APD/cam ratios vs. I/B